Progress In Electromagnetics Research Letters, Vol. 81, 51–58, 2019

Design of Continuous Polyharmonic-Tuned Power Amplifier with Optimal Knee Voltage Parameter

Gideon Naah*, Songbai He, and Weimin Shi

Abstract—This paper presents the design of a continuous polyharmonic-tuned mode (CPHTM) power amplifier (PA) with an introduced optimal knee voltage waveform control parameter in a continuous harmonic-tuned voltage waveform equation. The optimal knee voltage waveform control parameter works in unison with derived equations, providing bandwidth and efficiency potentials over the limiting factors of the conventional harmonic-tuned power amplifiers (PAs). The effectiveness of the design strategy is proven by the realisation of a CPHTM type-I (CPHTMT-I) PA as compared with a non-continuous polyharmonic-tuned mode type-II (NCPHTMT-II) PA. Test results with continuous-wave (CW) signals show drain efficiency (DE) levels within 53.6%–79% (1.31–2.39 GHz) with 58.4% fractional bandwidth for CPHTMT-I and 64%–78% (1.65–1.95 GHz) with 16.7% fractional bandwidth for NCPHTMT-II. The CW result evidently shows the validation and efficacy of the proposed theory.

1. INTRODUCTION

Wireless communication systems in this 21st century are deploying different varieties of power amplifiers (PAs) in their operations [1–21]. PAs operating within these wireless domains are required to be characterised by high efficiencies over a broad range of frequencies. Among these types of PAs are harmonic-tuned power amplifier (PA) and continuous PA mode [22–26].

Harmonic-tuning has been proven to have potentials in enhancing the performance of a PA by manipulating the PA's current and voltage waveforms but has bandwidth limitations as shown in [26] operating at a single frequency point.

In the case of continuous PA mode as in [23] which deals with finding the optimal design space, PA designers have devised various techniques in achieving at least the optimum Class B performance. [24] and [25] for example proposed continuous harmonic-tuned PAs based on inverse Class F and Class F PAs respectively. However, how the knee voltage influences the design and performance of continuous polyharmonic-tuned mode (CPHTM) PA was not considered. The effect of the knee voltage can dominate the whole design strategy of the continuous harmonic-tuned PA, thereby causing degradation in its performances. Thus, it must be investigated in order to find a suitable solution.

In this paper, as inspired by [24], an optimal knee voltage waveform control parameter with derived equations is proposed in designing a CPHTM PA possessing both polyharmonic-tuned and continuous mode properties. By this approach, a different voltage and bifurcated current waveforms are generated as compared with the related works [22, 24–26], enabling the designed PA to have better bandwidth and high efficiency characteristics than it was previously possible. Most importantly, the proposed strategy is validated with a devised CPHTM PA prototype. The proposed CPHTM PA's prototype has its operating frequency ranging from 1.31 to 2.39 GHz. The validity and efficacy of the proposed approach is vitally proved via the experimental results of the realised PA prototype with 58.4% fractional bandwidth

Received 28 September 2018, Accepted 21 November 2018, Scheduled 9 January 2019

* Corresponding author: Gideon Naah (engrgnaah7@gmail.com).

The authors are with the School of Electronic Science and Engineering, University of Electronic Science and Technology of China, Chengdu 611731, China.

and over 75% efficiency, 41 dBm output power, 15 dB gain, thus demonstrating high performance boost conferred by the design strategy.

2. DESIGN OF CONTINUOUS POLYHARMONIC-TUNED POWER AMPLIFIER WITH OPTIMAL KNEE VOLTAGE PARAMETER

Much has been said about continuous mode and harmonic-tuned PAs as presented in [22–26]. From a standard Class B and continuous modes' perspective, the current waveform (i.e., Equation (1)) of the Class B mode and voltage waveform (i.e., Equation (2)) of the continuous mode are shown for convenience as follows:

$$i_d(\theta) = I_{\max} \cdot \left(\frac{1}{\pi} + \frac{1}{2}\cos\theta + \frac{2}{3\pi}\cos 2\theta\right) \tag{1}$$

$$v_d(\theta) = V_{DD} \cdot (1 - \alpha\cos\theta + \beta\cos 3\theta) \cdot (1 - \gamma\sin\theta) \tag{2}$$

where $I_{\max}$ is the maximum current of the device in Equation (1); V_{DD} is the DC supply voltage; α, β determine the continuous mode; and γ regulates the range $(-1 \leq \gamma \leq 1)$ in Equation (2). By introducing a parameter V_k in Equation (2), Equation (2) becomes:

$$v_d^*(\theta) = (V_{DD} - V_k)(1 - \alpha\cos(\theta) + \beta\cos(3\theta)) \cdot (1 - \gamma\sin\theta) \tag{3}$$

where V_k represents the knee voltage of the device. Let us consider demarcating boundaries for the V_k operation labelled as lower (χ_B) and upper (μ_B) boundaries respectively. The subscript $_B$ denotes boundary in either case. Then, assign normalised values to χ_B and μ_B which are $\chi_B = 0.15$ and $\mu_B = 0.2$. In other words, χ_B and μ_B are normalised to unity. That is to say, χ_B and μ_B fall between 0 and 1 which are mathematically expressed in a unified form as $0 \leq \chi_B,\ \mu_B \leq 1$ with a step-size of 0.01. Furthermore, computations are performed using Equation (4), readily granting equal chances of yielding high performance to each boundary parameter. Additionally, the subsequent values for χ_B and μ_B which are 0.15 and 0.2 respectively, attained efficiency values greater than the conventional Class B PA mode which will be shown hereafter (see Fig. 2). Hence, these values are selected, and they are then normalised to V_{DD} represented as $\chi_B = 0.15\,V_{DD}$ and $\mu_B = 0.2\,V_{DD}$. Supposing that a parameter is introduced to control V_k and to ensure that it never moves beyond its predetermined range of operation and not for a moment graze zero, an optimal PA efficiency may be guaranteed. For convenience, this parameter is termed optimal knee voltage waveform control parameter denoted by δ. Hence, the derived and normalised equation for δ may be written as:

$$\delta = \chi_B\sqrt{2}\sin(\theta) + \mu_B\frac{1}{2}\cos(\theta). \tag{4}$$

Thus far, δ is derived to be used in the analysis, design, and implementation of the continuous polyharmonic-tuned mode type-I power amplifier (CPHTMT-I PA).

Assuming a PA having both polyharmonic-tuned and continuous mode properties derived from Equation (1) and Equation (3), and its voltage (i.e., Equation (5)) and current (i.e., Equation (6)) waveforms containing dc, fundamental and continuous polyharmonic components with Equation (4) introduced in Equation (5) can be expressed as:

$$v'_d(\theta) = (V_{DD} - \delta)(1 + \alpha\cos(\theta) + \beta\cos(2\theta) + \sigma\cos(3\theta) + \ldots) \cdot (1 - \gamma\sin(\theta)) \quad -1 \leq \gamma \leq 1 \tag{5}$$

$$i'_d(\theta) = \big(i_{DC} - i_1\cos(\theta) + i_2\cos(2\theta) + i_3\cos(3\theta) + \ldots\big) \cdot \big(1 - \gamma\sin(\theta)\big) \quad -1 \leq \gamma \leq 1 \tag{6}$$

where σ is the third harmonic voltage component variable in Equation (5), $i_{DC} = 0.37$, $i_1 = 0.43$, $i_3 = 0.06$ [23], and $i_2 = 0.156$ in Equation (6). From Equation (5), the influence of δ on the harmonic voltage components of the CPHTMT-I PA is derived and written as:

$$\begin{aligned} v''_d(\theta) = {} & (V_{DD} - \delta\alpha\cos(\theta)\gamma\sin(\theta) + \alpha\cos(\theta)\gamma\sin(\theta) - \delta\beta\cos(2\theta)\gamma\sin(2\theta) + \beta\cos(2\theta)\gamma\sin(2\theta) \\ & -\delta\sigma\cos(3\theta)\gamma\sin(3\theta) + \sigma\cos(3\theta)\gamma\sin(3\theta) - \delta\gamma\sin(4\theta) + \gamma\sin(4\theta)) \quad -1 \leq \gamma \leq 1. \end{aligned} \tag{7}$$

In order to prevent the resulting voltage from having a recursive effect back on the original current waveform should it drop below the knee voltage, the following conditions are required:

$$\begin{aligned} &\delta \in [0.15, \arcsin(\alpha, \beta, \sigma), && -1 \leq \gamma \leq 0.15 \\ &\delta \in (\arcsin(-(\alpha, \beta, \sigma)), 0.15], && 0.15 \leq \gamma \leq 1. \end{aligned} \tag{8}$$

As observed in Equation (7), the anti-phase requirement is achieved in all the harmonic voltage components while the conditions in Equation (8) strictly ensures the waveforms generated by Equation (7) never graze zero. With this phenomenon, maximum DC to RF conversion efficiency is much likely to be attained. In order to determine the coefficient variables in Equation (7), equate $\alpha = \frac{1}{\sqrt{2}}$, $\beta = \frac{1}{2}$, and $\sigma = \frac{1}{3\sqrt{3}}$. Then, it follows that the calculations are carried out beginning from the fundamental to the fourth harmonic voltage components with Equation (4) normalised; $\delta\alpha = 0.07071$, $\delta\beta = 0.05$, $\delta\sigma = 0.0192$, and $\delta\gamma = 1$. The resulting plot is shown in Fig. 1 using Equation (6) and Equation (7).

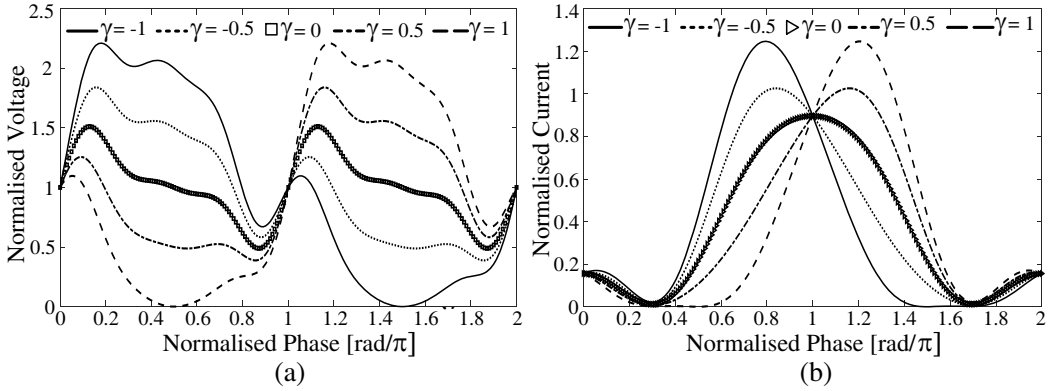

Figure 1. Normalised (a) voltage and (b) current waveforms.

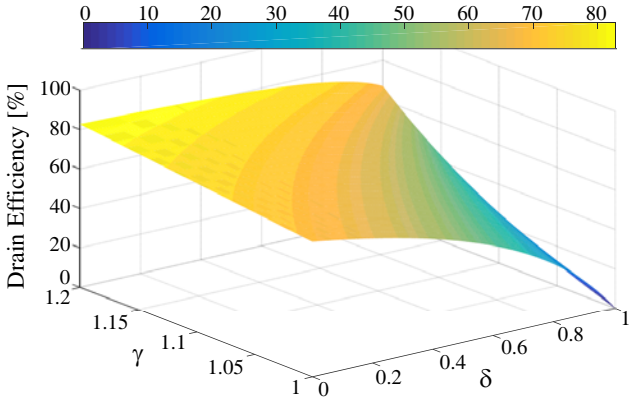

Figure 2. DE behaviour of δ. Note: The range for γ is further extended to examine the extent to which the δ can yield optimal performance.

From Equation (1), Equation (4), and Equation (7), the fundamental drain efficiency (DE) is derived as:

$$\eta = \frac{\pi}{4}\left(\frac{(\delta-\gamma)\left(\frac{1}{2\sqrt{4}}\sin(\theta)+\alpha\beta\sigma\cos(\theta)\right)}{-\sqrt{7}(\delta\gamma)}\right). \tag{9}$$

Equation (9) indicates a dependency on δ, γ, α, β, and σ. DE plot using Equation (9) is shown in Fig. 2, revealing that the theoretical DE behaviour due to the impacts the δ may have on the CPHTMT-I PA. At the point where $\delta = 0.15$ as evidently depicted, DE about 82.21% is recorded. Also, when $\delta = 0.2$, about 81.98% DE is reported. This phenomenon clearly indicates that, as δ increases, the V_{DD} is affected, degenerating the DE of the CPHTMT-I PA. Though the modified voltage waveforms appear at their peak points, the RF voltage swing is trying to drop below zero, causing a reduction of

the current waveforms at a point close to the peaks of the current. On the other hand, reducing the drive level will lead to an increment in the conduction angle, causing further DE deterioration in the CPHTMT-I PA. By the δ approach, a value of 0.1 is selected for the CPHTMT-I PA implementation. The selected δ value is of a realistic value for many practical cases, with the intent of the CPHTMT-I PA generating an optimal DE beyond that of the standard Class B PA mode.

Considerably, the harmonic components can also be expressed in the context of admittance presented below as fundamental (i.e., Equation (10a)), second (i.e., Equation (10b)), and third (i.e., Equation (10c)) harmonic admittances:

$$Y_{f_1} = \big(G_{opt}\sqrt{2}i_1 + jG_{opt}\sqrt{2}i_{DC}\big)\delta \tag{10a}$$

$$Y_{f_2} = \big(-jG_{opt}2\big(i_1 + i_2 + i_3\big)\big)\delta \tag{10b}$$

$$Y_{f_3} = \big(\infty\big)\delta \tag{10c}$$

G_{opt} defines the RF device's optimal conductance. The introduction of Equation (4) in Equation (10) is an indicator that all the harmonic components are dependent on δ in ensuring the attainment of high PA performances. This is achieved by δ positively impacting V_{DD}. By doing so, the suitable peak voltage and current waveforms required are triggered, leading to the reduction of high dc power consumption level. In spite of the i_2 inclusiveness, δ has a reasonable influence on the device, terminating in optimum system performance. This phenomenon is illustrated in Fig. 3 where Y_{f_1} and Y_{f_2} are almost positioned within the centre of the Smith chart, while an open circuit condition is presented by Y_{f_3}. The nearness of Y_{f_2} to that of Y_{f_1} is ascribed to the inclusiveness of the i_2. To this end, the method for achieving a CPHTM PA is presented and verified with normalised and idealised simulations.

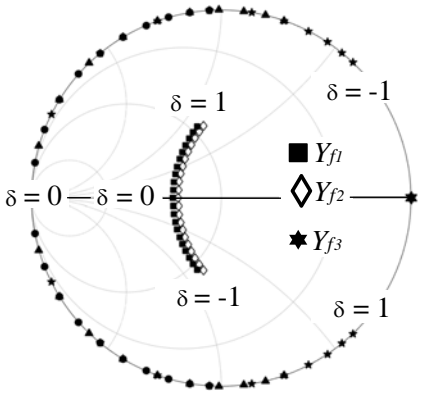

Figure 3. Admittance Smith chart acquired via Equation (10), indicating increased design space and broadband performance in the CPHTM PA. $-1 \leq \delta \leq 1$.

3. EXPERIMENTAL VALIDATION

Using a 10 W CGH40010F GaN HEMT device model produced by Wolfspeed, the CPHTMT-I PA was realised based on the preceding theory presented in Section 2. CPHTMT-I and NCPHTMT-II PAs operate at a frequency band of 1.31–2.39 GHz and 1.65–1.95 GHz, respectively. Both PAs were fabricated using Rogers' RO4350B substrate with $h = 30$ mil and $\varepsilon_r = 3.66$. They were also biased with the same $V_{GS} = -2.8$ V and $V_{DS} = 28$ V static bias points, quiescent current of 60 mA, $\delta = 0.1$, and fed with the same 29 dBm input power. These were done in order to make a fair comparison between the two solutions.

The selected $\delta = 0.1$ value is similar to a practical GaN device having a V_k of 4 V and working at 28 V DC supply. For the CPHTMT-I PA, its schematic, fabricated prototype, and nonlinear voltage-current waveforms at the current-generator plane supporting the theoretical ones in Fig. 1 are shown in Fig. 4, whereas those of the NCPHTMT-II PA are shown in Fig. 5.

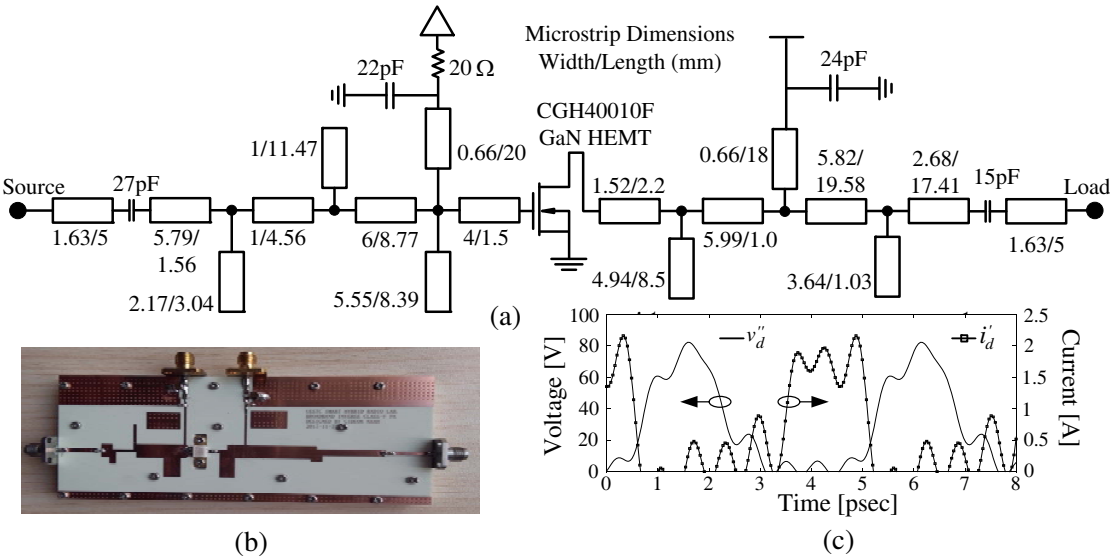

Figure 4. CPHTMT-I PA: (a) schematic, (b) fabricated prototype, (c) nonlinear current-generator plane v''_d and i'_d waveforms.

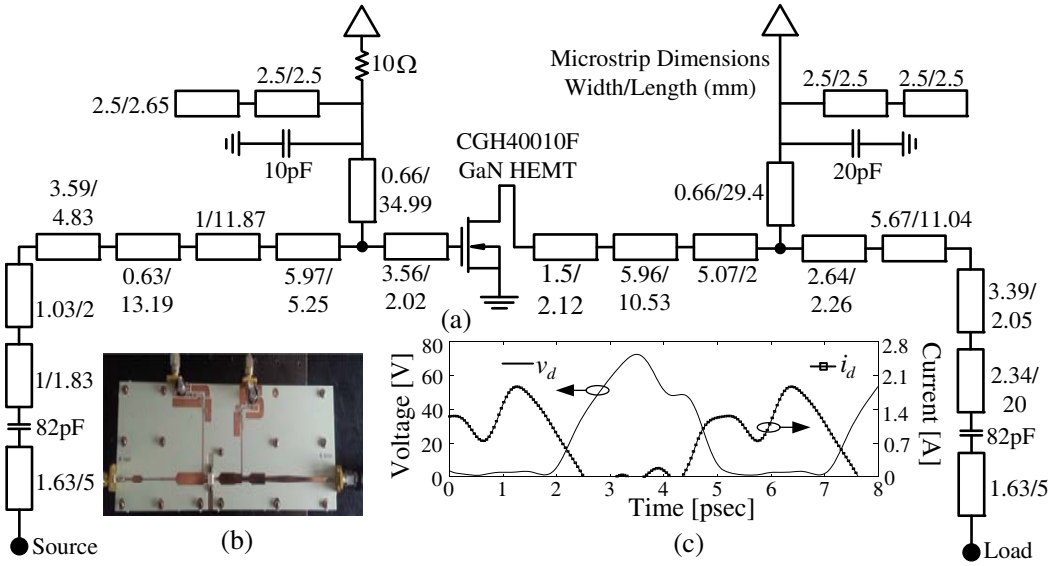

Figure 5. NCPHTMT-II PA: (a) schematic, (b) fabricated prototype, (c) nonlinear current-generator plane v_d and i_d waveforms.

The CPHTMT-I PA under continuous wave simulations successfully recorded 52.73%–81.18% DE, 40.84–42.69 dBm output power (Pout), and 11.84–13.69 dB gain shown in Fig. 6(a). At 2.38 GHz frequency, the maximum DE which is 81.18% was attained. This maximum DE improvement not only supports the theoretical DE behaviour reported in Fig. 2 but also clearly indicates a designed CPHTM PA whose performance is beyond that of the traditional Class B PA mode. The NCPHTMT-II PA under continuous wave simulations also recorded 71.4%–79.5% DE, 41.3–41.8 dBm Pout, and 14.8–15.3 dB gain illustrated in Fig. 6(b). Its maximum DE was acquired at 1.76 GHz frequency.

With continuous wave (CW) measurements, the CPHTMT-I PA recorded 53.6%–79% DE, 39.6–42.68 dBm Pout, and 12.6–16.96 dB gain as depicted in Fig. 6(a) whereas the NCPHTMT-II PA reported 64%–78% DE, 41–42 dBm Pout, and 13–17 dB gain as shown in Fig. 6(b). It is evidently shown in both simulations and measurements that the performance of the proposed CPHTMT-I PA has significantly

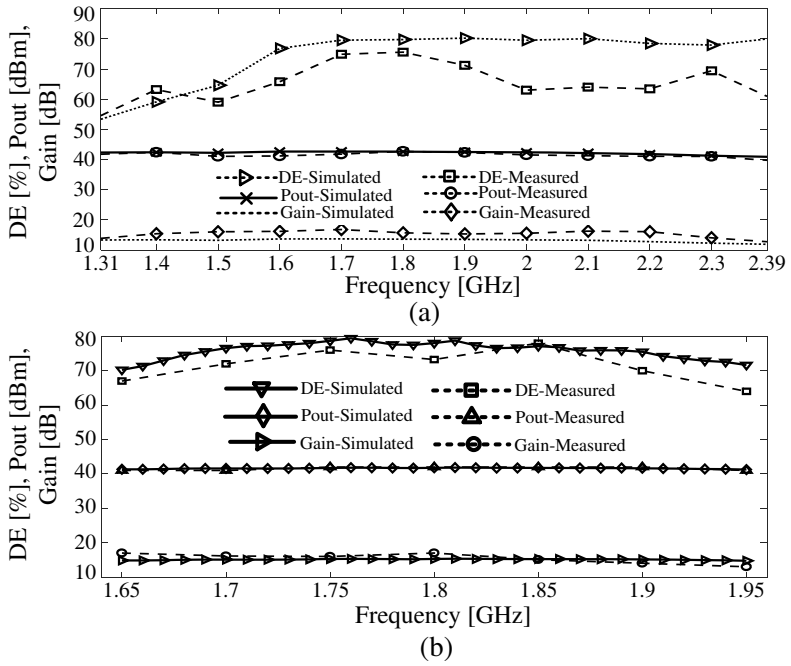

Figure 6. Measured and simulated results: (a) CPHTMT-I PA and (b) NCPHTMT-II PA.

Table 1. Comparison with some reported GaN harmonic PAs.

Ref.	Bandwidth (GHz) (%)	Pout (dBm)	Gain (dB)	DE (%)
2017 [22]	1.5–2.5 (50)	39.5–41.5	9.5–12.7	60–75
2015 [24]*	2.14 (-)	42.15	17.7	70.3
2016 [25]⋆	0.55–0.95 (53.3)	39–41	12–15	70–77
2018 [26]†	2.6 (-)	39.8	13	76
This work[1]	1.31–2.39 (58.4)	39.6–42.68	12.6–16.96	53.6–79
This work[2]	1.65–1.95 (16.7)	41–42	13–17	64–78

∗: $\gamma = 1$ are the compared PAs, ⋆: read from graph, †: GF $Z_{2fsource=j10\Omega}$,
[1]: CPHTMT-I PA, [2]: NCPHTMT-II PA.

improved over the performance of the NCPHTMT-II PA. The performance of the CPHTMT-I PA still extended well below the design band although there are discrepancies between measured and simulated results. The discrepancies may be attributed to the substrate material and complexity in the matching networks. The CPHTMT-I PA's test results are compared with some reported harmonic PAs as outlined in Table 1, suggesting the efficacy of the design approach.

4. CONCLUSION

A method for designing continuous polyharmonic-tuned mode power amplifier has been presented. For verification, a continuous polyharmonic-tuned mode type-I (CPHTMT-I) power amplifier prototype was implemented and compared with another implemented non-continuous polyharmonic-tuned mode type-II (NCPHTMT-II) power amplifier prototype. The experimental results clearly show more than 57% bandwidth and 78% efficiency in the CPHTMT-I power amplifier, indicating its superiority over the NCPHTMT-II power amplifier which has 16.7% bandwidth and 64%–78% efficiency, thus making the proposed power amplifier a potential candidate for modern wireless broadband systems.

REFERENCES

1. Zhou, X. Y., S. Y. Lee, W. S. Chan, S. Chen, and D. Ho, "Broadband efficiency-enhanced mutually coupled harmonic postmatching Doherty power amplifier," *IEEE Trans. Circuits Syst. I, Regular Papers*, Vol. 64, No. 7, 1758–1771, Jul. 2017.
2. Kim, J. H., S. J. Lee, B. H. Park, S. H. Jang, J. H. Jung, and C. S. Park, "Analysis of high-efficiency power amplifier using second harmonic manipulation: inverse class-F/J amplifiers," *IEEE Trans. Microw. Theory Tech.*, Vol. 59, No. 8, 2024–2036, Aug. 2011.
3. Stameroff, A. N., H. H. Ta, A. Pham, and R. E. Leoni III, "Wide-bandwidth power-combining and inverse class-F GaN power amplifier at X-band," *IEEE Trans. Microw. Theory Tech.*, Vol. 61, No. 3, 1291–1300, Mar. 2013.
4. Negra, R., A. Sadeve, S. Bensmida, and F. M. Ghannouchi, "Concurrent dual-band class-F load coupling network for applications at 1.7 and 2.14 GHz," *IEEE Trans. Circuits and Syst. II, Express Briefs*, Vol. 55, No. 3, 259–263, Mar. 2008.
5. Colantonio, P., F. Giannini, R. Giofrè, and L. Piazzon, "A design technique for concurrent dual-band harmonic tuned power amplifier," *IEEE Trans. Microw. Theory Tech.*, Vol. 56, No. 11, 2545–2555, Nov. 2008.
6. Chen, J., S. He, F. You, R. Tong, and R. Peng, "Design of broadband high-efficiency power amplifiers based on a series of continuous modes," *IEEE Microw. Wireless Compon. Lett.*, Vol. 24, No. 9, 631–633, Sept. 2014.
7. Xia, J., X. Zhu, and L. Zhang, "A linearized 2-3.5 GHz highly efficient harmonic-tuned power amplifier exploiting stepped-impedance filtering matching network," *IEEE Microw. Wireless Compon. Lett.*, Vol. 24, No. 9, 602–604, Sept. 2014.
8. Gao, L., X. Y. Zhang, S. Chen, and Q. Xue, "Compact power amplifier with bandpass response and high efficiency," *IEEE Microw. Wireless Compon. Lett.*, Vol. 24, No. 10, 707–709, Oct. 2014.
9. Chen, K. and D. Peroulis, "A 3.1-GHz class-F power amplifier with 82% power-added-efficiency," *IEEE Microw. Wireless Compon. Lett.*, Vol. 23, No. 8, 436–438, Aug. 2013.
10. Moon, J., S. Jee, J. Kim, J. Kim, and B. Kim, "Behaviors of class-F and class-F^{-1} amplifiers," *IEEE Trans. Microw. Theory Tech.*, Vol. 60, No. 6, 1937–1951, Jun. 2012.
11. Canning, T., P. Tasker, and S. Cripps, "Waveform evidence of gate harmonic short circuit benefits for high efficiency X-band power amplifiers," *IEEE Microw. Wireless Compon. Lett.*, Vol. 23, No. 8, 439–441, Aug. 2013.
12. Sharma, T., R. Darraji, and F. Ghannouchi, "A methodology for implementation of high-efficiency broadband power amplifiers with second-harmonic manipulation," *IEEE Trans. Circuits Syst. II, Express Briefs*, Vol. 63, No. 1, 54–58, Jan. 2016.
13. Huang, H., B. Zhang, C. Yu, J. Gao, Y. Wu, and Y. Liu, "Design of multioctave bandwidth power amplifier based on resistive second-harmonic impedance continuous class-F," *IEEE Microw. Wireless Compon. Lett.*, Vol. 27, No. 9, 830–832, Sept. 2017.
14. Morimoto, Y., et al., "A multiharmonic absorption circuit using quasi-multilayered striplines for RF power amplifiers," *IEEE Trans. Microw. Theory Tech.*, Vol. 65, No. 1, 109–118, Jan. 2017.
15. Hayati, M., A. Sheikhi, and A. Grebennikov, "Class-F power amplifier with high power added efficiency using bowtie-shaped harmonic control circuit," *IEEE Microw. Wireless Compon. Lett.*, Vol. 25, No. 2, 133–135, Feb. 2015.
16. Chen, K., T. Lee, and D. Peroulis, "Co-design of multi-band high-efficiency power amplifier and three-pole high-Q tunable filter," *IEEE Microw. Wireless Compon. Lett.*, Vol. 23, No. 12, 647–649, Dec. 2013.
17. Son, J., Y. Park, I. Kim, J. Moon, and B. Kim, "Broadband saturated power amplifier with harmonic control circuits," *IEEE Microw. Wireless Compon. Lett.*, Vol. 24, No. 3, 185–187, Mar. 2014.
18. Tuffy, N., L. Guan, A. Zhu, and T. J. Brazil, "A simplified broadband design methodology for linearized high-efficiency continuous class-F power amplifiers," *IEEE Trans. Microw. Theory Tech.*, Vol. 60, No. 6, 1952–1963, Jun. 2012.

19. Carrubba, V., et al., "On the extension of the continuous class-F mode power amplifier," *IEEE Trans. Microw. Theory Tech.*, Vol. 59, No. 5, 1294–1303, May 2011.
20. Chen, K. and D. Peroulis, "Design of broadband highly efficient harmonic-tuned power amplifier using in-band continuous class-F-1/F mode-transferring," *IEEE Trans. Microw. Theory Tech.*, Vol. 60, No. 12, 4107–4116, Dec. 2012.
21. Kim, J. H., G. D. Jo, J. H. Oh, Y. H. Kim, K. C. Lee, and J. H. Jung, "Modeling and design methodology of high-efficiency class-F and class-F^{-1} power amplifiers," *IEEE Trans. Microw. Theory Tech.*, Vol. 59, No. 1, 153–165, Jan. 2011.
22. Aggrawal, E., K. Rawat, and P. Roblin, "Investigating continuous class-F power amplifier using nonlinear embedding model," *IEEE Microw. Wireless Compon. Lett.*, Vol. 27, No. 6, 593–595, Jun. 2017.
23. Carrubba, V., et al., "Exploring the design space for broadband PAs using the novel continuous inverse class-F mode," *Proc. 41st Eur. Microw. Conf.(EuMC)*, 333–336, IEEE, Oct. 2011.
24. Merrick, B. M., et al., "The continuous harmonic-tuned power amplifier," *IEEE Microw. Wireless Compon. Lett.*, Vol. 25, No. 11, 736–738, Nov. 2015.
25. Sharma, T., et al., "Generalized continuous class-F harmonic tuned power amplifiers," *IEEE Microw. Wireless Compon. Lett.*, Vol. 26, No. 3, 213–215, Mar. 2016.
26. Sharma, T., et al., "High-efficiency input and output harmonically engineered power amplifiers," *IEEE Trans. Microw. Theory Tech.*, Vol. 66, No. 2, 1002–1014, Feb. 2018